

Magnetization of Iron Meteorites up to the Meter in Size as Possible Analogs for Asteroid Psyche



Key Points:

- The remanent magnetization of samples of individual iron meteorites decreases with size up to m^3 volumes, trending to a plateau value
- This plateau may correspond to the fraction of total magnetization due to minerals sharing a preferential magnetization direction, if any
- The remanent magnetization of asteroid (16) Psyche may be detectable depending on the magnitude of such a unidirectional component

Supporting Information:

Supporting Information may be found in the online version of this article.

Correspondence to:

C. Maurel,
cmaurel@cerege.fr

Citation:

Maurel, C., Clavé, E., Gattacecca, J., Uehara, M., Mansbach, E. N., McCoy, T. J., & Weiss, B. P. (2025). Magnetization of iron meteorites up to the meter in size as possible analogs for asteroid Psyche. *Journal of Geophysical Research: Planets*, 130, e2024JE008810. <https://doi.org/10.1029/2024JE008810>

Received 31 OCT 2024

Accepted 30 MAR 2025

Author Contributions:

Conceptualization: Clara Maurel, Benjamin P. Weiss

Data curation: Clara Maurel

Formal analysis: Clara Maurel, Elise Clavé

Funding acquisition: Benjamin P. Weiss

Investigation: Clara Maurel, Elise Clavé, Jérôme Gattacecca, Elias N. Mansbach, Timothy J. McCoy

Methodology: Clara Maurel, Elise Clavé, Jérôme Gattacecca, Minoru Uehara, Timothy J. McCoy, Benjamin P. Weiss

Resources: Timothy J. McCoy

Supervision: Benjamin P. Weiss

Clara Maurel^{1,2} , Elise Clavé^{1,3} , Jérôme Gattacecca² , Minoru Uehara² , Elias N. Mansbach¹ , Timothy J. McCoy⁴, and Benjamin P. Weiss¹ 

¹Department of Earth, Atmospheric and Planetary Sciences, Massachusetts Institute of Technology, Cambridge, MA, USA,

²CNRS, Aix Marseille University, IRD, INRAE, CEREGE, Aix-en-Provence, France, ³Deutsches Zentrum für Luft- und Raumfahrt (DLR), Institut für Optische Sensorsysteme, Berlin, Germany, ⁴Department of Mineral Sciences, National

Museum of Natural History, Smithsonian Institution, Washington, DC, USA

Abstract Meteorite paleomagnetic studies indicate planetesimal generated magnetic fields, but spacecraft magnetic measurements have yet to identify asteroidal natural remanent magnetization (NRM). This apparent discrepancy is of particular interest in the context of the NASA Psyche mission, which will search for evidence of past magnetic activity of the metal-rich asteroid (16) Psyche. Here, we aim to test whether the NRM of meteorites inevitably drops below detectable values as specimen size increases, which could explain why asteroidal NRMs could never be detected. We focus on iron meteorites as possible analogs to (16) Psyche's constituent material. To do so, we measure the remanent magnetic field and estimate the NRM of samples of four iron meteorites with volumes between mm^3 and m^3 . We find that their estimated NRMs decrease with increasing sample size but appear to plateau. These data are compatible with the idea that the bulk NRM of increasingly large objects becomes dominated by the fraction of this NRM produced by assemblages of magnetic minerals sharing a common magnetization direction. Moreover, all m^3 -sized meteorites carry NRMs that are two orders of magnitude above the detectability limit of the Psyche Magnetometer, three of which are possibly pre-terrestrial. These data, acquired on some of the largest masses of iron meteorites available on Earth, support the range of plausible NRM values for km-size regions of (16) Psyche, used to establish the spacecraft Magnetometer's performance requirements. Nevertheless, large-scale events such as brecciation of the asteroid following magnetization acquisition could always lower the asteroid's NRM below the detectability limit.

Plain Language Summary Asteroids and meteorites are fragments of planetesimals, the building blocks of planetary bodies. Laboratory studies of meteorite samples have shown that they contain remanent magnetization acquired in past magnetic fields. This indicates that, like the Earth, some planetesimals formed liquid metallic cores that generated these fields. In contrast, none of the seven spacecraft magnetic investigations at comets or asteroids have found reliable evidence for remanent magnetization. Searching for evidence of an ancient magnetic field is one of the objectives of the NASA Psyche mission that will orbit the metal-rich asteroid Psyche beginning 2029. Solving the apparent discrepancy between laboratory and spacecraft measurements is important for interpretation of the mission's future data. Here, we analyze the correlation between magnetization and sample size up to the meter-scale for iron meteorites, which are possible analogs of Psyche's constituent materials. Our data are compatible with the idea that, if the meteorite contains a fraction of magnetic minerals sharing a common magnetization direction, the bulk remanent magnetization of increasingly large specimens of this meteorite should reach a constant value. If asteroid Psyche is made of materials like known iron meteorites, it may therefore carry a magnetization detectable with the Psyche spacecraft Magnetometer.

1. Introduction

Meteorite paleomagnetic studies show that some planetesimals, planetary bodies of ~ 10 to 1,000 km in diameter that formed in the early solar system, internally generated dynamo magnetic fields (Scheinberg et al., 2015; Weiss et al., 2010). This dynamo activity was powered by the motion of a liquid metallic core within differentiated planetesimals (e.g., McCoy et al., 2006). The intensity and longevity of these magnetic fields reflect the physical properties of the source bodies, such as their size, core size and cooling history.

Ferromagnetic minerals in extraterrestrial rocks that experience such a dynamo field while either cooling or crystallizing will acquire a magnetic moment preferentially aligned with the direction of the field. A stronger

© 2025. The Author(s).

This is an open access article under the terms of the [Creative Commons Attribution-NonCommercial-NoDeriv](https://creativecommons.org/licenses/by/4.0/) License, which permits use and distribution in any medium, provided the original work is properly cited, the use is non-commercial and no modifications or adaptations are made.

Visualization: Clara Maurel
Writing – original draft: Clara Maurel
Writing – review & editing:
 Clara Maurel, Elise Clavé,
 Jérôme Gattacceca, Minoru Uehara, Elias
 N. Mansbach, Timothy J. McCoy,
 Benjamin P. Weiss

ambient field will result in the magnetic moments of more crystals being preferentially aligned. For the right conditions of size, shape, composition and crystal structure of the minerals, this alignment will persist over the age of the solar system (Lappe et al., 2011; Mansbach et al., 2022; Shah et al., 2017). The ferromagnetic minerals (a) whose magnetic moments were subsequently misaligned by remagnetization or brecciation events, or (b) that cooled/crystallized before the emergence or after the extinction of the dynamo field, will not share a preferential direction of their magnetic moments.

The natural remanent magnetization (NRM) of a rock is the volume-normalized vector sum of all the magnetic moments of its ferromagnetic minerals: the fraction of unidirectionally oriented magnetic moments, if any, and the remaining fraction of non-unidirectionally oriented ones. To provide a statistically robust record of the ancient field, the number of grains carrying the unidirectional fraction must exceed a threshold depending on the fidelity of the NRM record. This number is estimated to 1–10 billion but depends on the nature of the mineral assemblage (Berndt et al., 2016); it is easily reached in natural samples formed in typical planetary dynamo fields ($>10 \mu\text{T}$). The unidirectional fractions of extraterrestrial NRMs provide records of the magnetic environment and/or geological evolution of planetesimals. Any material carrying an NRM generates a remanent magnetic field that extends into space around it. Measurements of this field can be used to estimate the total magnetic moment and thus the bulk NRM of the rock.

Our understanding of planetesimal magnetic activity has been predominantly derived from laboratory analyses of the NRM carried on meteorites at the millimeter, micrometer and nanometer scales (e.g., Bryson, Herrero-Albillos et al., 2014; Gattacceca & Rochette, 2004; Lima & Weiss, 2016). Magnetic measurements conducted directly on asteroids can offer a complementary perspective on the astrophysical and geological context in which planetesimals formed and evolved. Spacecraft magnetometers have measured the magnetic fields surrounding six asteroids and a comet to search for evidence of remanent magnetization. The total intrinsic magnetic field of an asteroid, if any, is the combination of a remanent components formed by a past magnetic field (e.g., dynamo) superposed on a field induced by the interplanetary magnetic field. The field can be described using a spherical harmonic expansion, with the first-degree terms describing the dipole contribution and higher-degree terms describing multipole contributions. Because of the rapid decay of higher-degree terms with distance from the field source, an onboard magnetometer will measure a dominantly dipolar field at large distances. Once the induced component is removed, the spherical harmonic expansion of the remanent field is used to estimate the remanent magnetic moment, either of the bulk asteroid or of a localized region, depending on the spatial resolution of the measurements. Strong NRMs ($\sim 10^{-2} \text{ A m}^2 \text{ kg}^{-1}$) were tentatively inferred from the flybys of asteroids (951 Gaspra and (9969) Braille by the Galileo and Deep Space 1 spacecraft, respectively (Kivelson et al., 1993; Richter et al., 2001). However, the perturbations associated with the solar wind magnetic field and/or instrument noise may have been the source of the measured signals (Blanco-Cano et al., 2003; Herčík et al., 2020). The other five small bodies visited by spacecraft—asteroids (21) Lutetia and (2867) Šteins (flybys (Auster et al., 2010; Richter et al., 2012)), (433) Eros (orbiter (Acuña et al., 2002)), comet 67P/Churyumov-Gerasimenko and asteroid (162173) Ryugu (landers (Auster et al., 2015; Herčík et al., 2020))—did not have a detectable remanent field.

New asteroid magnetic measurements are anticipated with the NASA Psyche mission (Weiss et al., 2023). Beginning 2029, the Psyche spacecraft will orbit asteroid (16) Psyche, the largest metal-rich asteroid of the asteroid Main Belt. This object may contain between ~ 30 and ~ 60 vol.% metal given its estimated density of $3,400\text{--}4,100 \text{ kg m}^{-3}$ (Elkins-Tanton et al., 2020). The primary goal of the mission is to determine whether the asteroid formed from the metallic core of a planetesimal that lost most of its silicate mantle during repeated stripping impacts. In this scenario, Psyche's outermost material could potentially have acquired a NRM while being exposed to magnetic fields internally generated by its molten interior (Figures 1a and 1b) (Elkins-Tanton et al., 2022). The Magnetometer onboard the Psyche spacecraft was designed to detect a remanent field of at least 1.5 nT (Weiss et al., 2023). This detectability limit corresponds to a scenario where Psyche is composed of boulders of 40 km in diameter, each with a bulk NRM of $10^{-4} \text{ A m}^2 \text{ kg}^{-1}$, oriented randomly (Figure 1c (Weiss et al., 2023)). The intensity of this NRM is based on measurements conducted on ~ 100 iron meteorite samples with sizes <10 cm (Terho et al., 1993). This model therefore assumes that km-size boulders could carry an NRM of the same intensity as that measured on cm-size samples.

There is an apparent discrepancy between the lack of compelling evidence for asteroids with remanent fields and the large number of extraterrestrial NRMs interpreted as records of a dynamo activity on meteorite parent bodies. The absence of detectable asteroid-scale remanent magnetization has been attributed to at least two causes. First,

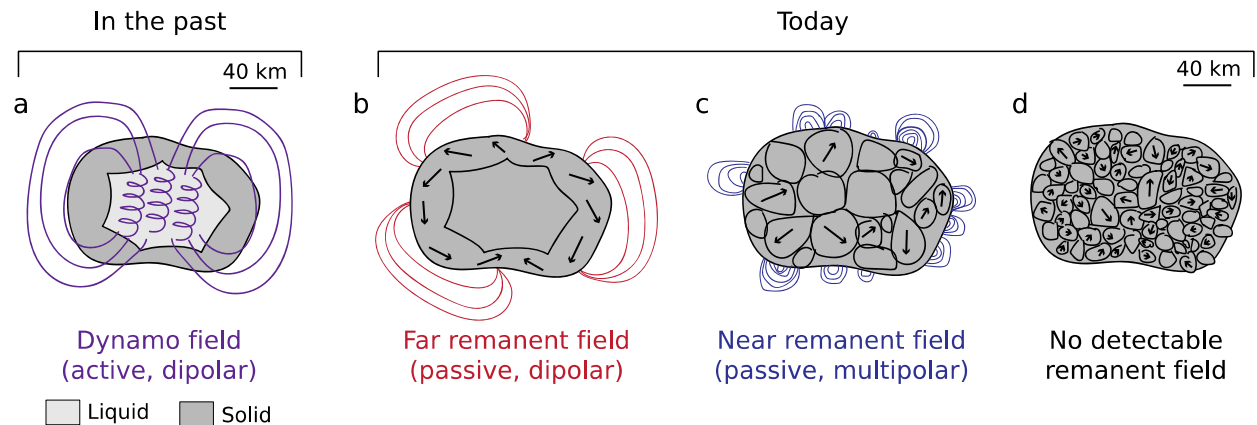


Figure 1. Schematics of possible natural remanent magnetizations (NRMs) and remanent fields at (16) Psyche. (a) All scenarios illustrated here assume that the asteroid once generated an active, short-lived dynamo field that magnetized its outer layer (Elkins-Tanton et al., 2022). (b) Remanent magnetization (black arrows) of the asteroid if it did not undergo any destructive collision posterior to magnetization acquisition. The Psyche Magnetometer could detect far fields (likely dipolar, red lines) produced by the NRM of km-size regions. (c) Remanent magnetization (black arrows) of the asteroid if it was destroyed and reaccumulated, spatially randomizing >40-km-sized blocks magnetized carrying a unidirectional NRM fraction. Near remanent fields (likely multipolar, black lines) produced by the resultant of the NRM of the blocks could be detectable as long as the NRM of individual blocks is $>10^{-4} \text{ A m}^2 \text{ kg}^{-1}$. This scenario was adopted to set the lower detection limit of the Psyche Magnetometer (Weiss et al., 2023). (d) Remanent magnetization of the asteroid if it is now an agglomerate of small boulders (rubble pile; not necessarily at scale on the figure). The boulders were re-oriented randomly during collisional grinding and their resultant magnetization did not produce fields measurable at spacecraft altitudes.

the asteroids visited by spacecraft may simply not have experienced or generated a substantial magnetic field, as suggested for comet 67P (Biersteker et al., 2019) and asteroid Ryugu (Mansbach et al., 2024; Maurel et al., 2024), in which case they would never have acquired a detectable NRM. Second, some of these asteroids may be made of smaller regions carrying a NRM with possibly varying NRM directions, but either their NRM is too weak, and/or their directions are sufficiently scattered that their net magnetic fields are undetectable at spacecraft altitudes (e.g., Figure 1d) (Wasilewski et al., 2002).

We do not know which of the scenarios in Figure 1, if any, will apply to (16) Psyche. Here, we propose to test—in the limits of what is feasible prior to the arrival of the spacecraft—two assumptions highlighted in the previous paragraphs. First, because iron meteorites are possible analogs to (16) Psyche's constituent material, the weakest magnetic field required to be detectable by Psyche's Magnetometer was determined based on the assumption that km-size, iron-meteorite-like blocks can have NRMs of the same intensity as cm-size iron meteorites ($>10^{-4} \text{ A m}^2 \text{ kg}^{-1}$ (Weiss et al., 2023)). Here, we test this hypothesis using a series of remanent field measurements conducted on specimens between 10^{-2} and 10^{-1} m^3 in volume, some of the largest masses of iron meteorites available on Earth. Second, by estimating the resultant NRM of samples of the same meteorite at different sizes (mm^3 to m^3), we aim to test whether the NRM of iron meteorites inevitably decreases with increasing size due to the random orientation of its constituent magnetized units (Wasilewski et al., 2002). Aside from the first meteorite ever measured magnetically (Anyzeski, 1949), only one other iron meteorite specimen has ever been measured in the 10^{-2} m^3 size range (Wasilewski et al., 1997). Size-dependent measurements have only been conducted on four chondritic meteorites (size range: 10^{-9} m^3 to 10^{-3} m^3 (Wasilewski et al., 2002)).

2. Model, Samples and Methods

In this section, we propose a simple model to predict how the magnetization of an object may change with size. We also describe the selected meteorites and our experimental methods.

2.1. Magnetization as a Function of Volume

Asteroids and meteorites exposed to ancient steady fields such as a dynamo field may contain a fraction of ferromagnetic minerals sharing a common preferential orientation of their magnetic moments. This preferential magnetization direction may also postdate arrival on Earth, and may result from (a) the acquisition of a viscous remanent magnetization (VRM) during a prolonged exposure to the geomagnetic field, (b) the acquisition of a chemical remanent magnetization (CRM) by ferromagnetic iron oxides, formed by alteration of meteoritic metal

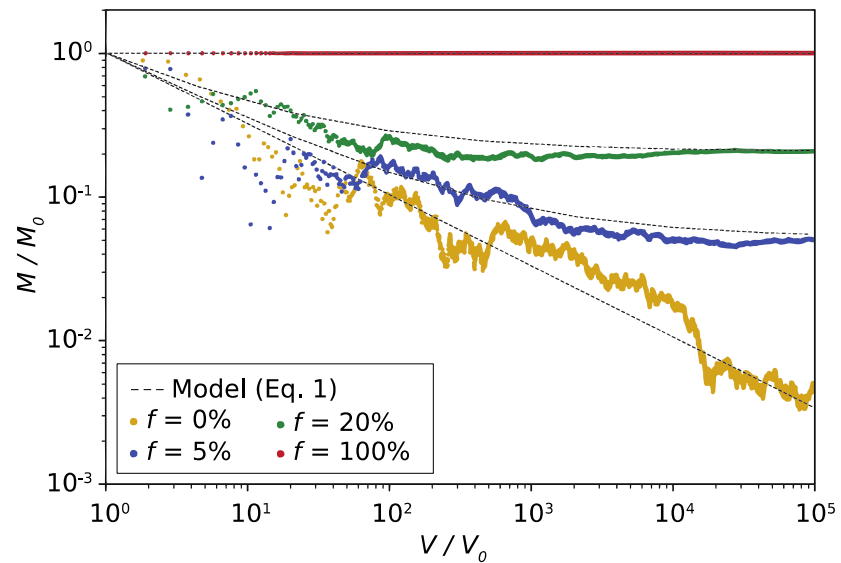


Figure 2. Volume-normalized magnitude of the resultant of unit vectors, M , as a function of the sum of associated unit volumes, V . Both quantities are normalized to those of a single unit vector, M_0 , or volume, V_0 . Dashed lines show the outcome of Equation 1 for different fractions of unidirectionally oriented vectors, f . Dots show the outcome of the simulation for the same values of f .

in the terrestrial environment, and/or (c) the acquisition of an isothermal remanent magnetization by exposure to a magnet or possibly lightning.

We propose a qualitative model in which the remanent magnetization of an object is represented by the sum of unit vectors oriented unidirectionally, and unit vectors oriented randomly. The former represent the magnetic moments of the ferromagnetic crystals or domains that were magnetized by a steady field, which we call the “unidirectional component” of the remanent magnetization. The latter represent the magnetic moments of the remaining ferromagnetic crystals or domains. In nature, a rock may be exposed to multiple magnetizing fields, and may thus contain multiple ensembles of ferromagnetic minerals sharing distinct preferential directions (i.e., have a multidirectional remanence). For simplicity, however, we only consider here the case of a single unidirectional NRM component. Furthermore, the model does not account for any magnetic interactions between the vectors that might partially reorient them. These interactions can be strong at the nanoscale (Blukis et al., 2020) and are part of the NRM of bulk samples. At the mm scale and larger, however, interactions between magnetic minerals in iron meteorites can result in “self-demagnetization” only if the sample has been exposed to artificial magnetic fields much stronger than planetary fields (Figure S1 in Supporting Information S1).

The number of unit vectors is gradually increased to simulate the increasing volume of a sample. Doing so, we choose to keep the fraction of unidirectionally oriented vectors (f) constant. This is equivalent to assuming that increasingly large specimens of the same meteorite are homogenous in magnetic mineralogy and experienced the same magnetizing field. The model calculates the magnitude of the resultant of all the unit vectors contained in a volume $V = NV_0$ where V_0 is a unit volume of magnetization M_0 . The relationship between the volume-normalized magnitude of the resultant, M , and the volume can then be parametrized as (Figure 2):

$$\frac{M}{M_0} = f + (1-f)\sqrt{\frac{V_0}{V}} \quad (1)$$

In Equation 1, the two extreme cases where $f = 1$ and $f = 0$ replicate well-known results: if all vectors are unidirectionally oriented ($f = 1$), M is constant and equal to M_0 for all N and V ; if all vectors are randomly oriented ($f = 0$), their resultant decreases as $1/\sqrt{N}$, or equivalently, M decreases as $1/\sqrt{V}$. If $0 < f < 1$, M decreases with increasing V and asymptotes to fM_0 , because the resultant of the randomly oriented vectors tends to zero, while the resultant of the unidirectionally oriented vectors is constant (Figure 2). As such, according to this model, if we were to measure increasingly large specimens of the same object—all of them being

Table 1
Natural Remanent Magnetization (NRM) and Saturation Remanent Magnetization, M_{rs} , for Samples of Casas Grandes, Cranbourne, Navajo and Quinn Canyon in the mm^3 , 0.1-cm^3 (Cranbourne, Navajo) and m^3 Size Ranges

Meteorite	Group	Mass (kg)	Volume (m^3)	NRM ($\text{A m}^2 \text{kg}^{-1}$)	M_{rs} ($\text{A m}^2 \text{kg}^{-1}$)	Magnet overprint?
Casas Grandes	IIIAB	24.5×10^{-6}	3.14×10^{-9}	3.22×10^{-2}	0.394	No
		16.1×10^{-6}	2.06×10^{-9}	3.21×10^{-2}	–	No
		12.1×10^{-6}	1.55×10^{-9}	2.74×10^{-2}	–	No
		750	9.61×10^{-2}	$(1.5 \pm 0.3) \times 10^{-3}$	–	–
Cranbourne	IAB	26.6×10^{-6}	3.41×10^{-9}	5.26×10^{-2}	0.061	Yes
		0.87×10^{-3}	1.11×10^{-7}	9.53×10^{-4}	–	–
		1.90×10^{-3}	2.43×10^{-7}	1.81×10^{-3}	–	–
		4.35×10^{-3}	5.58×10^{-7}	4.78×10^{-4}	–	–
	591	7.58×10^{-2}	$(9.5 \pm 2.5) \times 10^{-4}$	–	–	
Navajo	IIAB	33.7×10^{-6}	4.32×10^{-9}	2.33×10^{-2}	0.229	Maybe
		18.3×10^{-6}	2.34×10^{-9}	2.21×10^{-2}	–	Maybe
		15.8×10^{-6}	2.02×10^{-9}	8.6×10^{-3}	–	Maybe
		1.89×10^{-3}	2.42×10^{-7}	1.62×10^{-2}	–	–
	633	8.12×10^{-2}	$(11.2 \pm 0.03) \times 10^{-3}$	–	–	
Quinn Canyon	IIIAB	24.3×10^{-6}	3.11×10^{-9}	2.75×10^{-3}	0.240	No
		20.8×10^{-6}	2.67×10^{-9}	4.53×10^{-3}	–	No
		21.7×10^{-6}	2.78×10^{-9}	10.4×10^{-3}	–	No
		460	5.90×10^{-2}	$(1.6 \pm 1.0) \times 10^{-3}$	–	–

Note. Columns 3 to 6 give the mass, estimated volume, NRM and M_{rs} (of the mm^3 sized samples), respectively. In column 7, we indicate whether the sample was likely contaminated by a magnet. The uncertainty of the NRM for m^3 samples is a 95% confidence interval.

homogenous in magnetic mineralogy and having experienced the same magnetizing field—their NRM as a function of volume should reach a plateau equal to the intensity of its unidirectional component. In other words, at some sufficiently large value of V , the NRM as a function of V should follow a trend with a slope shallower than $1/\sqrt{V}$.

2.2. Selected Samples and Magnetic Mineralogies

We analyzed four different meteorites from three groups that are thought to represent three different parent planetesimals: Casas Grandes and Quinn Canyon (IIIAB group), Navajo (IIAB group), and Cranbourne (IAB group), with sample volumes ranging from mm^3 to m^3 (Table 1). The volumes of each sample were estimated using the sample mass and the average density of iron meteorites, $\sim 7,800 \text{ kg m}^{-3}$ (Consolmagno & Britt, 2013). Samples were obtained from the Smithsonian National Museum of Natural History and the Museum National d’Histoire Naturelle de Paris.

Major ferromagnetic minerals in these samples include kamacite ($\text{Fe}_{1-x}\text{Ni}_x$ with $x < 0.06 \text{ wt.}\%$), taenite ($\text{Fe}_{1-x}\text{Ni}_x$ with $\sim 0.25 < x < 0.5 \text{ wt.}\%$), tetrataenite (ordered $\text{Fe}_{1-x}\text{Ni}_x$ with $x \sim 50 \text{ wt.}\%$), schreibersite [$(\text{Fe},\text{Ni}_3)\text{P}$] and cohenite (Fe_3C) (Goldstein et al., 2009). Kamacite and taenite/tetrataenite can form intergrowths of a few tenths of mm to several mm in size (Widmanstätten pattern) and of hundreds of nm to μm in size (plessite). Inside the Ni-rich regions of the Widmanstätten pattern, taenite/tetrataenite forms (a) μm -thick “clear rims,” and (b) “cloudy zones” with $< 0.2\text{-}\mu\text{m}$ taenite/tetrataenite grains (Goldstein et al., 2009). In some iron meteorites, tetrataenite in cloudy zones is a potent magnetization carrier that can preserve its NRM for billions of years (Bryson, Church, et al., 2014; Einsle et al., 2018; Uehara et al., 2011). Finally, kamacite that experienced peak shock pressures $> 13 \text{ GPa}$ exhibits a visibly distorted, recrystallized aspect, commonly called ϵ -kamacite. This is due to a transient change in the crystal structure of the kamacite, followed by a reverse transformation to its initial ferromagnetic structure.

Casas Grandes (7.7 wt.% Ni) and Quinn Canyon (8.40 wt.% Ni) are structurally similar medium octahedrites with long kamacite lamellae of 1.1–1.15 mm in width. Plessite occupies 35%–40% of the surface of $\sim 0.5\text{-m}^2$ examined sections (Buchwald, 1975). Schreibersite is present in both specimens and exhibits shearing and displacement, likely due to mild shock (<12 GPa). Like other IIIAB meteorites, Casas Grandes and Quinn Canyon are likely to contain sub-micrometer Ni-rich tetrataenite grains (in clear rims, cloudy zones and plessite (Yang & Goldstein, 2006)).

Navajo has 5.5 wt.% Ni and is a coarse octahedrite with cm-sized Ni-poor kamacite fingers and ϵ -kamacite. Sub-mm sized schreibersite and cohenite grains are present. Buchwald (1975) suggested that large planar sections might reveal Ni-rich taenite. However, the Old Woman IAB meteorite (higher Ni content and similar P content compared to Navajo) was found to lack Ni-rich taenite during optical examination of $\sim\text{m}^2$ surfaces (Plotkin et al., 2012). Ni in Navajo may therefore be concentrated in schreibersite, leaving ϵ -kamacite as the only Fe-Ni phase potentially carrying a magnetic remanence.

Cranbourne has 7.0 wt.% Ni and is a coarse octahedral pattern with kamacite lamellae 2–4 mm in width and ϵ -kamacite. Plessite fields and taenite ribbons with widths of tens of μm are present along with inclusions of graphite, troilite, schreibersite and cohenite (typical for IAB irons; Buchwald, 1975). The largest mass is covered by limonite, a non-magnetic mineral formed by terrestrial weathering. Like other IAB meteorites, Cranbourne may also contain tetrataenite in cloudy zones and plessite. A paleomagnetic investigation of two IAB iron meteorites suggests, however, that at the time tetrataenite formed in the IAB meteorites, their parent body was not generating a dynamo magnetic field (Nichols et al., 2018).

2.3. Remanence Measurements

All magnetic measurements were conducted at the Massachusetts Institute of Technology (MIT, USA) and the Center de Recherche et d'Enseignement des Geosciences de l'Environnement (CEREGE, France). We measured the NRM of up to four specimens per meteorite in the $\text{mm}^3/0.1\text{-cm}^3$ range that did not have apparent rust or remains of a fusion crust. For this, we used a 2G Superconducting Rock Magnetometer 755 equipped with automated degaussing and remagnetization coils (Kirschvink et al., 2008) inside a magnetically shielded room (ambient field intensity <200 nT). The mm^3 samples were subjected to stepwise three-axis alternating field demagnetization up to 140 mT. We also estimated their saturation remanent magnetization (M_{rs}) (the maximum remanent magnetization that a sample can acquire) after applying a 1-T spatially uniform magnetic field to the samples using a Princeton Micromag vibrating sample magnetometer. We also, for comparison, measured the NRM of all the iron meteorites available in the CEREGE meteorite collection. For the specimens that were too big to fit in the 2G magnetometer, we used a Molspin Minispin magnetometer.

NRM demagnetization data and M_{rs} can help identify a magnetic contamination by contact with a hand magnet, which is recognizable if the direction of the NRM vector as it demagnetizes describes a curved trajectory and/or if the NRM/M_{rs} ratio exceeds $\sim 10\%$ (Vervelidou et al., 2023). For comparison, a basalt that acquired a thermoremanent magnetization in the Earth field (~ 50 μT) has a NRM/M_{rs} ratio of 1%–2% (Gattacceca & Rochette, 2004).

Another type of contamination of the NRM is the gradual acquisition of a VRM after a prolonged exposure to the geomagnetic field (Yu & Tauxe, 2006). To quantify the contribution of a room-temperature VRM to the total remanence, we conducted VRM acquisition and decay experiments on samples of Casas Grandes, Navajo, Quinn Canyon (all demagnetized to 140 mT prior to the experiment) and Cranbourne (not demagnetized). To measure the VRM acquisition rate (r_a), we kept the samples in a 57- μT field (B_{lab}) oriented along the x axis and regularly measured their magnetic moments. With the exception of Casas Grandes, acquisition experiments were conducted on two samples per meteorite. To measure the VRM decay rate (r_d), we placed the samples in a $<50\text{-nT}$ field and regularly measured their magnetic moments. Both rates are estimated using a linear regression of the measured remanence as a function of the logarithm of time (Yu & Tauxe, 2006). To estimate a maximum VRM acquired (VRM_{max}), we assume the samples were kept stationary in a steady field (B_{Earth}) of 45 μT for their entire residence time on Earth (t), which we assume is $\sim 10,000$ years (e.g., the terrestrial age of the largest iron meteorite on Earth, Hoba, is less than 80,000 years (McCorkell et al., 1968)): $\text{VRM}_{\text{max}} = (r_a/B_{\text{lab}}) \log_{10}(t) B_{\text{Earth}}$.

We analyzed four m^3 specimens directly at the Museum Support Center of the Smithsonian National Museum of Natural History. We measured their remanent magnetic field using a magnetometer array designed to

accommodate and measure the remanent magnetic field of large specimens in an unshielded environment. A detailed description of the instrument and the measurement sequence are given in Clavé et al. (2020). The parameters of the system are given in Table S1 in Supporting Information S1. The magnetometer consists of two pairs of orthogonal square Helmholtz coils and four magnetometers mounted on a movable aluminum rail. The Helmholtz coils are manually oriented to generate a magnetic field aligned with the background magnetic field. The meteorite is taken in and out of the instrument using a forklift. With and without the meteorite inside, the intensity of the generated field is gradually increased to partially compensate the background field up to a maximum. The rail is sequentially placed on the four sides and on top of the sample zone such that the magnetic field inside the system was measured at 20 different locations at a minimum distance of one equivalent sample radius (Figure S2 in Supporting Information S1). The difference between the field measured by the fluxgates with and without the meteorite provides a measurement of the meteorite's total field (which is the sum of the induced and remanent fields). As the intensity of the field applied by the coils decreases, the induced fraction of the meteorite's total field weakens, while its remanent fraction remains constant. A linear regression between each component of the meteorite's total field and the norm of the applied field provides an estimate of the remanent field at the 20 positions of the fluxgates.

The magnetic moment of the sample is estimated using the spherical harmonics algorithm presented by Clavé et al. (2020). For the 20 positions, the three components of the remanent field are taken as inputs of a nonlinear regression with Tikhonov regularization to search for the optimal origin of the expansion before solving for the spherical harmonics coefficients and estimating the magnetic moment (Text S1 in Supporting Information S1). Clavé et al. (2020) tested the analysis pipeline on the same Nd-Fe-B magnet with a total magnetic moment of $8.05 \pm 0.15 \text{ A m}^2$ and were able to retrieve the moment within 5% of its true value using an expansion of degree $N = 6$. We used the same parameters to estimate the magnetic moment of the meteorites. To estimate the uncertainty on the magnetic moment, the time series of measurements recorded by each fluxgate were sampled with replacement before using these values for the linear regression. This operation was repeated 100 times to obtain a 95% confidence interval.

3. Results

NRM data are summarized in Table 1 and Figure 3. For comparison, the NRM measured on the samples of the CEREGE meteorite collection are summarized in Table S2 in Supporting Information S1; here we focus on the four selected meteorites. The average NRM of the mm^3 samples ranges between $5.9 \times 10^{-3} \text{ A m}^2 \text{ kg}^{-1}$ (Quinn Canyon) and $5.3 \times 10^{-2} \text{ A m}^2 \text{ kg}^{-1}$ (Cranbourne). The NRM of the 0.1-cm^3 samples of Cranbourne and Navajo ranges between $4.8 \times 10^{-4} \text{ A m}^2 \text{ kg}^{-1}$ and $1.6 \times 10^{-2} \text{ A m}^2 \text{ kg}^{-1}$. With $\text{NRM}/M_{rs} \sim 40\%$, the mm^3 sample of Cranbourne was likely magnetically contaminated. This ratio drops to $\sim 1\%$ for the 0.1-cm^3 samples of the same meteorite. Navajo, Casas Grandes and Quinn Canyon have $\text{NRM}/M_{rs} \sim 7.8\%$, 7.7% and 2.4% , respectively. Their demagnetization data do not exhibit a curved trajectory typical of magnetic contamination, possibly at the exception of Navajo (Figure S3 in Supporting Information S1). We also measured the M_{rs} of Cranbourne for sample sizes between 5 and 500 mm^3 . Because M_{rs} is the maximum remanent magnetization a sample can acquire, Equation 1 predicts that M_{rs} should not vary significantly with sample size if the magnetic mineralogy is homogenous across samples. Our data validate this prediction, at least for Cranbourne (Figure 3).

The ratio of VRM acquisition rate to VRM decay rate ranges between 1.1 and 3.7 depending on the meteorite (Table 2). Although Néel's theory predicts a ratio between 1 and 2 depending on the grain magnetic states (Néel, 1949), a slower decay rate than the acquisition rate is commonly seen (Fabian & Shcherbakov, 2018). The fact that these ratios are not too far off the theoretical range supports the reliability of our data. Extrapolating the VRM acquisition to 10,000 years (Section 2.3), we find a maximum VRM ranging between $1.7 \times 10^{-4} \text{ A m}^2 \text{ kg}^{-1}$ (Quinn Canyon) and $9.0 \times 10^{-3} \text{ A m}^2 \text{ kg}^{-1}$ (Cranbourne) (Figures S4 and S5 in Supporting Information S1). This maximum VRM represents 4%, 10%, 14%, and 950% of the NRM of the m^3 samples of Navajo, Quinn Canyon, Casas Grandes and Cranbourne, respectively.

The multipole inversion model proposed by Clavé et al. (2020) for m^3 sized samples (Figure 4; Figures S6–S8 in Supporting Information S1) yielded NRM estimates ranging between $(9.5 \pm 2.5) \times 10^{-4} \text{ A m}^2 \text{ kg}^{-1}$ (Cranbourne) and $(1.12 \pm 0.03) \times 10^{-2} \text{ A m}^2 \text{ kg}^{-1}$ (Navajo). This range encompasses the only published NRM estimate for a 474-kg sample of the iron meteorite Canyon Diablo ($1.72 \times 10^{-3} \text{ A m}^2 \text{ kg}^{-1}$; Wasilewski et al., 1997).

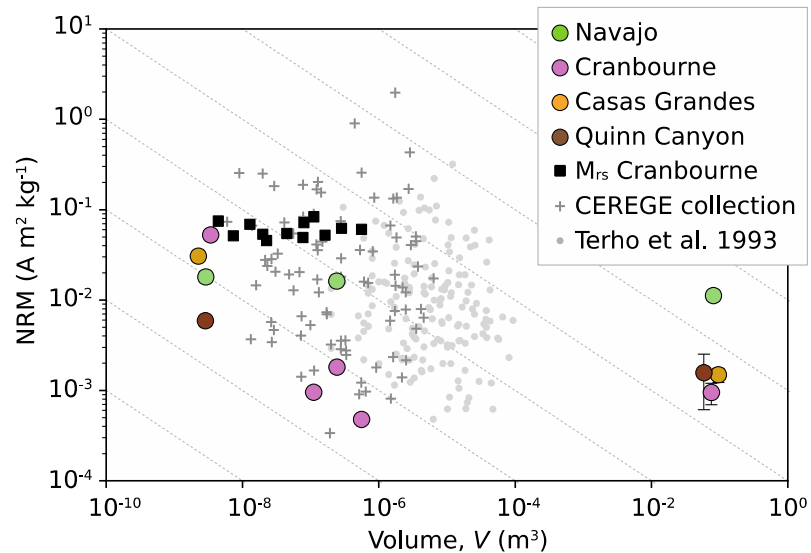


Figure 3. Natural remanent magnetization (NRM) as a function of volume. Filled colored circles show NRM measured for the four selected meteorites (the NRM is averaged over the three mm^3 samples). Gray crosses show the NRM of all iron-meteorite samples in the CEREGE collection (Table S2 in Supporting Information S1), and gray dots show data from Terho et al. (1993). Squares show the saturation remanent magnetization of subsamples of the meteorite Cranbourne. Dashed gray lines have a slope proportional to $1/\sqrt{V}$. Error bars of m^3 samples are a 95% confidence interval.

4. Discussion

4.1. Magnetization as a Function of Size

Between mm^3 and m^3 volumes, the NRM of Casas Grandes, Navajo and Quinn Canyon decrease by a factor of 20, 2 and 4, respectively. For Cranbourne, the NRM of the 0.1-cm^3 , while somewhat scattered, are within uncertainty of those of the m^3 samples. If the NRM of the meteorites was only carried by ensembles of ferromagnetic minerals that do not share a preferential direction of their magnetic moments (i.e., absence of unidirectional NRM component), a $1/\sqrt{V}$ line should pass through the 95% confidence intervals of all data points of a given meteorites, which is not observed (Section 2.1; Figure 3). Despite the limited data available, this suggests that the NRM of these four meteorites has a unidirectional NRM component. The relatively flat trend of Navajo, Quinn Canyon and Cranbourne could even indicate that their NRMs are at a plateau (Figures 2 and 3) and can be considered spatially coherent above the cm scale.

To understand the potential origin of such a unidirectional NRM component, we consider the possibility that the samples were magnetized after arrival on Earth (e.g., magnetically contaminated) versus before arrival (e.g., potentially preserving a record acquired on their parent body). With respect to the former, there are several

Table 2
VRM Acquisition and Decay Parameters

Meteorite	Mass (mg)	Acquisition rate, r_a ($\text{A m}^2 \text{kg}^{-1} \log(\text{t})^{-1}$)	Decay rate, r_d ($\text{A m}^2 \text{kg}^{-1} \log(\text{t})^{-1}$)	r_a/r_d	VRM 10^4 years ($\text{A m}^2 \text{kg}^{-1}$)
Casas Grandes	19.1	2.35×10^{-5}	-8.81×10^{-6}	2.7	$<2.1 \times 10^{-4}$
Cranbourne	419	7.98×10^{-4}	-5.81×10^{-4}	1.4	$<7.2 \times 10^{-3}$
	1,900	9.91×10^{-4}	–	1.7*	$<9.0 \times 10^{-3}$
Navajo	33.7	4.50×10^{-5}	-1.21×10^{-5}	3.7	$<4.1 \times 10^{-4}$
	1,885	2.76×10^{-5}	–	2.3*	$<2.5 \times 10^{-4}$
Quinn Canyon	36.2	1.86×10^{-5}	-1.73×10^{-5}	1.1	$<1.7 \times 10^{-4}$
	67.2	4.97×10^{-5}	–	2.9*	$<4.5 \times 10^{-4}$

Note. Columns 1 and 2 list the meteorite name and mass. Columns 3 and 4 give the acquisition and decay rates (r_a and r_d , respectively). Column 5 lists the r_a/r_d ratio (*indicates the rates were not estimated using the same specimen). Column 6 is the estimated VRM acquired over 100,000 years assuming a $45\text{-}\mu\text{T}$ steady ambient field.

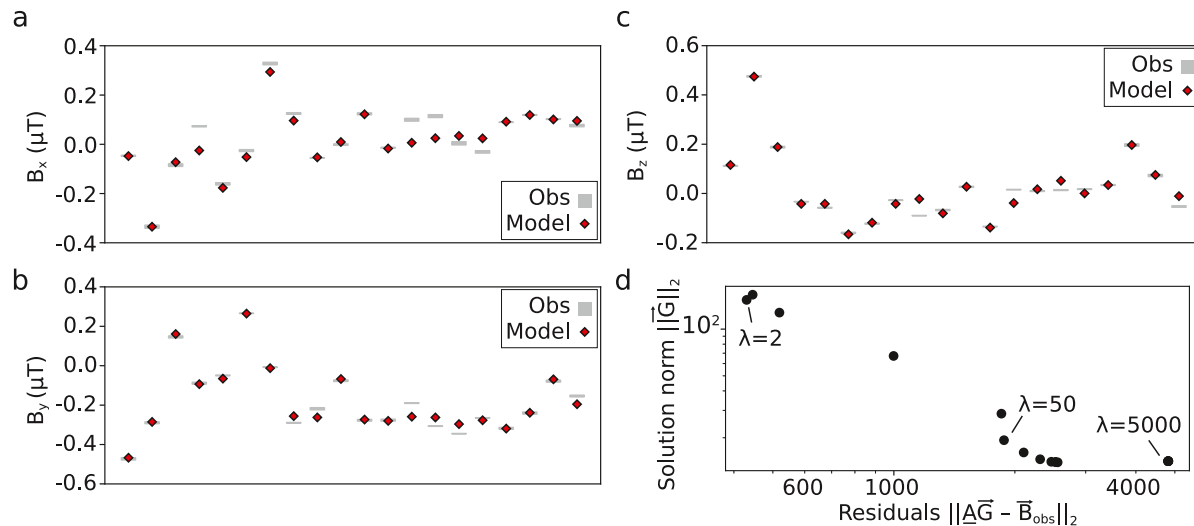


Figure 4. Measured remanent magnetic field, forward model and magnetic moment retrieval for the m^3 sample of Casas Grandes. (a–c) Measured remanent magnetic field and its 95% confidence interval recorded at each of the 20 sensor positions is shown by gray symbols. The model field is shown by red diamonds. (d) L-curve resulting from the minimization of Equation S6 (see Supporting Information S1). The value of $\lambda = 50$ was used to calculate the model field in panels (a–c).

common sources of such magnetic contamination. First, the reheating of the outer layer during atmospheric entry and acquisition of a partial thermoremanent magnetization is unlikely to account for a significant fraction of the measured NRM (Text S2; Table S3 in Supporting Information S1). Moreover, during their fall, the maximum tensile pressure experienced by meteorites occurs upon entering the atmosphere and is estimated at <5 MPa (Borovička et al., 2020), which is too low to have any demagnetizing effect on their NRM (Bezaeva et al., 2010). Second, to avoid a potential CRM contamination, we only selected $\text{mm}^3/0.1\text{-cm}^3$ samples without apparent signs of terrestrial alteration. The m^3 specimens, given their size and lack of porosity, are unlikely to be rusted deeper than their surface. Third, although contact with a cm-sized magnet would have affected the NRM of mm^3 or 0.1-cm^3 samples, it would have contributed very little to the NRM of m^3 samples given that the field of a cm-sized magnet is reduced to an intensity of a few mT at a distance of ~ 10 cm (Vervelidou et al., 2023). Multiple magnet applications might have partially randomized the magnetization direction of the meteorite's exterior but they should not have affected the interior of the m^3 specimens. Finally, a VRM acquired in the geomagnetic field could partially or totally explain the unidirectional component of the NRM of at least Cranbourne—in this case, the estimated upper limit on the VRM acquired is larger than the measured NRM for m^3 samples (Table 2). Because none of these potential sources of magnetic contamination seem to explain the NRM of Quinn Canyon, Casas Grandes and Navajo across the explored volume range, this suggests that the unidirectional component of their NRM possibly predates their arrival on Earth. Additional data are needed to confirm this hypothesis.

Altogether, our data are compatible with the idea that the intensity of the NRM estimated for increasingly large iron meteorite samples (sharing the same homogenous mineralogy and magnetic history) eventually becomes equal to the intensity of the unidirectional component of this NRM. Multiple factors likely influence the threshold size at which this occurs, including the quantity and nature of stable magnetization carriers and the magnetic history of the meteorite, and we cannot place constraints on this threshold. Interestingly, Navajo is an extreme example where the NRM can be almost constant at least up to the m^3 , despite the fact that the meteorite does not host tetrataenite, which is commonly thought to be a major carrier of stable remanence in many iron meteorites. Our data, acquired on specimens of different meteorite groups, suggest that iron meteorites at least up to a meter in size can carry a detectable NRM despite their differences in bulk mineralogies.

4.2. Implications for Spacecraft Measurements and the Psyche Mission

The requirement for the Psyche Magnetometer is to be able to measure a remanent field produced by Psyche's outer layer at a distance of 85 km from the surface (about one Psyche radius (Polanskey et al., 2018)), assuming the layer is composed of randomly oriented boulders with a spatial coherence of 40 km and minimum magnetization of 10^{-4} A m^2 kg^{-1} (Weiss et al., 2023). In this case, the minimum detectable bulk magnetization of the

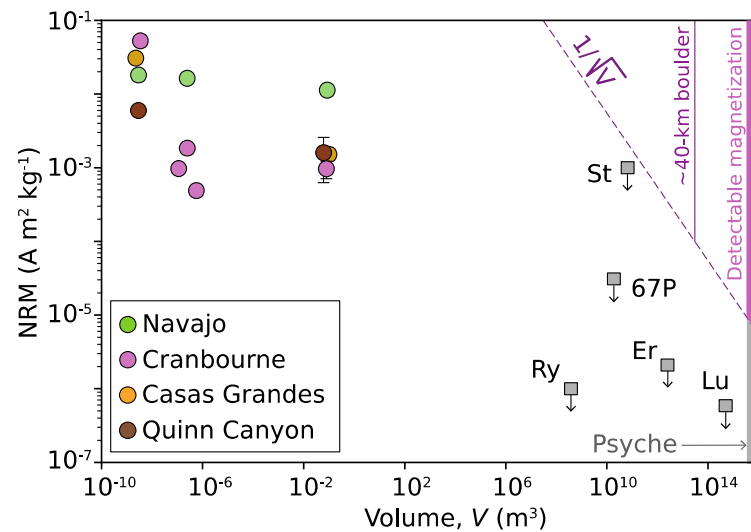


Figure 5. NRM as a function of volume. Colored circles show the four meteorites analyzed in this study. Squares show the upper limits on the bulk magnetization estimated for the asteroids/comets visited by a spacecraft carrying a magnetometer. The thick vertical line indicates the approximate volume of asteroid (16) Psyche. The Psyche Magnetometer is designed to detect a remanent magnetization resulting from ~ 40 -km diameter boulders with a minimum magnetization of $10^{-4} \text{ A m}^2 \text{ kg}^{-1}$ (thin vertical line) that are spatially randomly oriented. Following a $1/\sqrt{V}$ line (dashed line), this yields a minimum detectable bulk magnetization of $\sim 10^{-5} \text{ A m}^2 \text{ kg}^{-1}$ for Psyche (pink thick line). St: Šteins, 67P: 67P/Churyumov-Gerasimenko, Ry: Ryugu, Er: Eros, Lu: Lutetia.

asteroid would be $\sim 10^{-5} \text{ A m}^2 \text{ kg}^{-1}$ (Figure 5). Numerical simulations of interactions between a magnetized Psyche and the solar wind conducted to investigate the field geometries that might be encountered at the asteroid are also based on a bulk magnetization range of 10^{-5} to $10^{-2} \text{ A m}^2 \text{ kg}^{-1}$ (Oran et al., 2022). In comparison, our data show that the remanent field of m^3 meteorites—probably the largest analogs of Psyche's material on Earth for which we will be able to estimate a NRM—remains largely detectable by fluxgate magnetometers placed about two sample radii away from the surface. The magnetization of these m^3 samples is above $\sim 10^{-3} \text{ A m}^2 \text{ kg}^{-1}$, and at least for Navajo, Cranbourne and Quinn Canyon, does not substantially vary at least across the explored size scales. The lower limit for detectability of the Psyche Magnetometer is therefore still largely below the estimated NRM of meter-size iron meteorites.

The detectability of a unidirectional NRM component at the km scale from spacecraft data will depend on the nature and volume fraction of the magnetic carriers and on the intensity of the magnetizing field. Tetraenite in cloudy zones has a saturation remanent magnetization of $60 \text{ A m}^2 \text{ kg}^{-1}$ (Dos Santos et al., 2015). Assuming that the NRM of cloudy zones is 1% of their M_{rs} (similar to a basalt magnetized in the geomagnetic field (Gattacceca & Rochette, 2004)) and that cloudy zones are the only unidirectionally magnetized structures, a bulk magnetization of $10^{-4} \text{ A m}^2 \text{ kg}^{-1}$ would imply that cloudy zones occupy a minimum fraction of 0.02 vol.% of the total magnetized volume, which is compatible with meteorites that exhibit a Widmanstätten pattern (Buchwald, 1975). By contrast, the IAB Navajo provides an example of a meteorite dominated by Ni-poor kamacite that does not have cloudy zones.

So far, we have considered objects that are homogenous in composition and homogeneously magnetized throughout their entire volume. This is unlikely to directly apply to an entire asteroid, but could reflect regions with a fraction of their NRM unidirectionally oriented (Figure 1). Comparisons of the outcomes of numerical simulations with the maximum spatial resolution achievable by the Psyche spacecraft (40 km) will be essential to determine whether the NRM of the layer can be estimated. Finally, the idea that the unidirectional fraction of the NRM will tend to dominate the signal of the bulk NRM as specimen size increases (potentially up to the km scale, assuming homogenous mineralogy and common magnetic history) should apply to asteroids other than metal-rich ones, as long as they experienced ancient magnetic fields and their resulting NRM was not fully randomized, for example, by brecciation and reaccretion after collisions.

5. Conclusion

We estimated the NRM of four iron meteorites at different size scales: $\text{mm}^3/0.1\text{-cm}^3$ and m^3 . All four meteorites carry a non-zero NRM at least up to the m^3 . The NRM as a function of volume does not decay as steeply as expected if the meteorites were only carrying ensembles of ferromagnetic minerals that do not share a preferential direction of their magnetic moments (assuming a homogenous magnetic mineralogy and magnetic history among the different pieces). This suggests that a fraction of the meteorites' NRM is unidirectional. For at least one meteorite, the IAB Cranbourne, a VRM acquired in the Earth field is the likely dominant source of this remanence, making it less relevant to asteroidal magnetism. On the other hand, for the IIIAB meteorites Quinn Canyon, Casas Grandes and the IIAB Navajo, we cannot readily explain their NRM as the result of terrestrial contamination, suggesting that part of their NRM possibly predates their arrival on Earth. Additional data are needed to confirm this hypothesis.

Our data are compatible with the hypothesis that, for increasingly large volumes homogeneously magnetized, the unidirectional fraction of their NRM will dominate the estimated remanence, while the intensity of the remaining fraction—resulting from ensembles of ferromagnetic minerals that do not share a preferential direction of their magnetic moments—will tend to zero. This appears to be applicable to a range of iron meteorite mineralogy. The detectability of the NRM of an asteroid (or part of an asteroid) that was exposed to an ancient magnetic field should therefore only depend on the intensity of this unidirectional fraction of the NRM, controlled by the magnetic mineralogy and the intensity of the ancient magnetizing field. In addition, our data show that the NRMs of m^3 -sized iron meteorites—probably the largest Psyche analogs that will be measured on Earth—are still largely detectable by a fluxgate magnetometer. This further supports the magnetization range employed to simulate potential field geometries and intensities at asteroid (16) Psyche.

Conflict of Interest

The authors declare no conflicts of interest relevant to this study.

Data Availability Statement

All data needed to evaluate the conclusions in the paper can be found on the Zenodo repository (Maurel et al., 2025).

Acknowledgments

We thank the Smithsonian Institution and the Museum National d'Histoire Naturelle for the loan of the samples. We thank Julie Hoskin for granting us access to the meteorites of the Museum Support Center of the Smithsonian Museum of Natural History, Richard Stoyer and Daniella Haigler for their precious help with the logistics. We thank Kathryn Rowe, Henry Gonzalez, and Roger Fu for their MEDA fluxgate magnetometers; Eduardo Lima, Foteini Vervelidou and Yoann Quesnel for helpful discussions on the dipole and multipole inversion models. C. M., B. P. W. and E. C. thank the NASA Discovery Program (grant NNM16AA09C), the MIT International Science and Technology Initiatives (MISTI) and T. F. Peterson, Jr. for support. C. M. and J. G. thank the ANR funding program for support (grant ANR-23-CE49-0010).

References

- Acuña, M. H., Anderson, B. J., Russell, C. T., Wasilewski, P., Kletetschka, G., Zanetti, L., & Omid, N. (2002). NEAR magnetic field observations at 433 Eros: First measurements from the surface of an asteroid. *Icarus*, 155(1), 220–228. <https://doi.org/10.1006/icar.2001.6772>
- Anyzeski, V. (1949). The possible significance of magnetism in meteorites. In *Popular astronomy* (pp. 249–250).
- Auster, H. U., Apathy, I., Berghofer, G., Fornacon, K.-H., Remizov, A., Carr, C., et al. (2015). The nonmagnetic nucleus of comet 67P/Churyumov-Gerasimenko. *Science*, 349(6247), aaa5102. <https://doi.org/10.1126/science.aaa5102>
- Auster, H. U., Richter, I., Glassmeier, K. H., Berghofer, G., Carr, C. M., & Motschmann, U. (2010). Magnetic field investigations during ROSETTA's 2867 Šteins flyby. *Planetary and Space Science*, 58(9), 1124–1128. <https://doi.org/10.1016/j.pss.2010.01.006>
- Berndt, T., Muxworthy, A. R., & Fabian, K. (2016). Does size matter? Statistical limits of paleomagnetic field reconstruction from small rock specimens. *Journal of Geophysical Research, [Solid Earth]*, 121(1), 15–26. <https://doi.org/10.1002/2015jb012441>
- Bezaeva, N. S., Gattacceca, J., Rochette, P., Sadykov, R. A., & Trukhin, V. I. (2010). Demagnetization of terrestrial and extraterrestrial rocks under hydrostatic pressure up to 1.2GPa. *Physics of the Earth and Planetary Interiors*, 179(1), 7–20. <https://doi.org/10.1016/j.pepi.2010.01.004>
- Biersteker, J. B., Weiss, B. P., Heinisch, P., Herčík, D., Glassmeier, K.-H., & Auster, H.-U. (2019). Implications of Philae magnetometry measurements at comet 67P/Churyumov-Gerasimenko for the nebular field of the outer solar system. *The Astrophysical Journal*, 875(1), 39. <https://doi.org/10.3847/1538-4357/ab0f2a>
- Blanco-Cano, X., Omid, N., & Russell, C. T. (2003). Hybrid simulations of solar wind interaction with magnetized asteroids: Comparison with Galileo observations near Gaspra and Ida. *Journal of Geophysical Research*, 108(A5), 1216. <https://doi.org/10.1029/2002ja009618>
- Blukis, R., Pfau, B., Günther, C. M., Hessing, P., Eisebitt, S., Einsle, J., & Harrison, R. J. (2020). Nanoscale imaging of high-field magnetic hysteresis in meteoritic metal using X-ray holography. *Geochemistry, Geophysics, Geosystems*, 21(8). <https://doi.org/10.1029/2020gc009044>
- Borovička, J., Spurný, P., & Šhrbený, L. (2020). Two strengths of ordinary chondritic meteoroids as derived from their atmospheric fragmentation modeling. *The Astronomical Journal*, 160(1), 42. <https://doi.org/10.3847/1538-3881/ab9608>
- Bryson, J. F. J., Church, N. S., Kasama, T., & Harrison, R. J. (2014). Nanomagnetic intergrowths in Fe–Ni meteoritic metal: The potential for time-resolved records of planetesimal dynamo fields. *Earth and Planetary Science Letters*, 388, 237–248. <https://doi.org/10.1016/j.epsl.2013.12.004>
- Bryson, J. F. J., Herrero-Albillos, J., Kronast, F., Ghidini, M., Redfern, S. A. T., van der Laan, G., & Harrison, R. J. (2014). Nanopaleomagnetism of meteoritic Fe–Ni studied using X-ray photoemission electron microscopy. *Earth and Planetary Science Letters*, 396, 125–133. <https://doi.org/10.1016/j.epsl.2014.04.016>
- Buchwald, V. F. (1975). *Handbook of iron meteorites*. University of California Press.

- Clavé, E., Maurel, C., Lima, E. A., Shah, J., Mansbach, E. N., Uehara, M., & Weiss, B. P. (2020). A portable magnetometer for magnetic measurements of meter-sized meteorites. *Geochemistry, Geophysics, Geosystems*, 21(11), e2020GC009266. <https://doi.org/10.1029/2020GC009266>
- Consolmagno, G. J., & Britt, D. T. (2013). Iron meteorite density and heat capacity. *76th Annual Meteoritical Society Meeting*, 5, 5128.
- Dos Santos, E., Gattacceca, J., Rochette, P., Scorzelli, R. B., & Fillion, G. (2015). Magnetic hysteresis properties and 57Fe Mössbauer spectroscopy of iron and stony-iron meteorites: Implications for mineralogy and thermal history. *Physics of the Earth and Planetary Interiors*, 242, 50–64. <https://doi.org/10.1016/j.pepi.2015.01.004>
- Einsle, J. F., Eggeman, A. S., Martineau, B. H., Saghi, Z., Collins, S. M., Blukis, R., et al. (2018). Nanomagnetic properties of the meteorite cloudy zone. *Proceedings of the National Academy of Sciences of the United States of America*, 115(49), E11436–E11445. <https://doi.org/10.1073/pnas.1809378115>
- Elkins-Tanton, L. T., Asphaug, E., Bell, J. F., 3rd, Bierson, C. J., Bills, B. G., Bottke, W. F., et al. (2022). Distinguishing the origin of asteroid (16) Psyche. *Space Science Reviews*, 218(3), 17. <https://doi.org/10.1007/s11214-022-00880-9>
- Elkins-Tanton, L. T., Asphaug, E., BellBercoviciBills, J. F. H. B., Bercovici, H., Bills, B., Binzel, R., et al. (2020). Observations, meteorites, and models: A preflight assessment of the composition and formation of (16) Psyche. *Journal of Geophysical Research: Planets*, 125(3), e2019JE006296. <https://doi.org/10.1029/2019je006296>
- Fabian, K., & Shcherbakov, V. P. (2018). Energy barriers in three-dimensional micromagnetic models and the physics of thermoviscous magnetization. *Geophysical Journal International*, 215(1), 314–324. <https://doi.org/10.1093/gji/ggy285>
- Gattacceca, J., & Rochette, P. (2004). Toward a robust normalized magnetic paleointensity method applied to meteorites. *Earth and Planetary Science Letters*, 227(3), 377–393. <https://doi.org/10.1016/j.epsl.2004.09.013>
- Goldstein, J. I., Scott, E. R. D., & Chabot, N. L. (2009). Iron meteorites: Crystallization, thermal history, parent bodies, and origin. *Chemie der Erde*, 69(4), 293–325. <https://doi.org/10.1016/j.chemer.2009.01.002>
- Herčík, D., Auster, H.-U., Constantinescu, D., Blum, J., Fornaçon, K.-H., Fujimoto, M., et al. (2020). Magnetic properties of asteroid (162173) ryugu. *Journal of Geophysical Research: Planets*, 125(1), e2019JE006035. <https://doi.org/10.1029/2019je006035>
- Kirschvink, J. L., Kopp, R. E., Raub, T. D., Baumgartner, C. T., & Holt, J. W. (2008). Rapid, precise, and high-sensitivity acquisition of paleomagnetic and rock-magnetic data: Development of a low-noise automatic sample changing system for superconducting rock magnetometers. *Geochemistry, Geophysics, Geosystems*, 9(5), Q05Y01. <https://doi.org/10.1029/2007gc001856>
- Kivelson, M. G., Bargatze, L. F., Khurana, K. K., Southwood, D. J., Walker, R. J., & Coleman, P. J., Jr. (1993). Magnetic field signatures near Galileo's closest approach to Gaspra. *Science*, 261(5119), 331–334. <https://doi.org/10.1126/science.261.5119.331>
- Lappe, S.-C. L. L., Church, N. S., Kasama, T., da Silva Fanta, A. B., Bromiley, G., Dunin-Borkowski, R. E., et al. (2011). Mineral magnetism of dusty olivine: A credible recorder of pre-accretionary remanence. *Geochemistry, Geophysics, Geosystems*, 12(12), Q12Z35. <https://doi.org/10.1029/2011gc003811>
- Lima, E. A., & Weiss, B. P. (2016). Ultra-high sensitivity moment magnetometry of geological samples using magnetic microscopy. *Geochemistry, Geophysics, Geosystems*, 17(9), 3754–3774. <https://doi.org/10.1002/2016gc006487>
- Mansbach, E. N., Shah, J., Williams, W., Maurel, C., Bryson, J. F. J., & Weiss, B. P. (2022). Size ranges of magnetic domain states in tetraenaite. *Geochemistry, Geophysics, Geosystems*, 23(11), e2022GC010631. <https://doi.org/10.1029/2022gc010631>
- Mansbach, E. N., Weiss, B. P., Lima, E. A., Sowell, M., Kirschvink, J. L., Fu, R. R., et al. (2024). Evidence for magnetically-driven accretion in the distal solar system. *AGU Advances*, 5(6), e2024AV001396. <https://doi.org/10.1029/2024av001396>
- Maurel, C., Clavé, E., Gattacceca, J., Uehara, M., Mansbach, E. N., McCoy, T. J., & Weiss, B. P. (2025). Magnetization of iron meteorites up to the meter scale as possible analogs for asteroid Psyche [Dataset]. *Zenodo*. <https://doi.org/10.5281/zenodo.14018243>
- Maurel, C., Gattacceca, J., & Uehara, M. (2024). Hayabusa 2 returned samples reveal a weak to null magnetic field during aqueous alteration of Ryugu's parent body. *Earth and Planetary Science Letters*, 627, 118559. <https://doi.org/10.1016/j.epsl.2023.118559>
- McCorkell, R. H., Fireman, E. L., D'Amico, J., & Thomson, S. O. (1968). Radioactive isotopes in Hoba West and other iron meteorites. *Meteoritics*, 4(2), 113–122. <https://doi.org/10.1111/j.1945-5100.1968.tb00378.x>
- McCoy, T. J., Mittlefehldt, D. W., & Wilson, L. (2006). Asteroid differentiation. In S. Dante & H. Y. McSween Jr (Eds.), *Meteorites and the early solar system II* (pp. 733–745). Univ. of Arizona Press.
- Néel, L. (1949). Théorie du traînage magnétique des ferromagnétiques en grains fins avec application aux terres cuites. *Annales de Geophysique*, 5, 99–136.
- Nichols, C. I. O., Krakow, R., Herrero-Albillos, J., Kronast, F., Northwood-Smith, G., & Harrison, R. J. (2018). Microstructural and paleomagnetic insight into the cooling history of the IAB parent body. *Geochimica et Cosmochimica Acta*, 229, 1–19. <https://doi.org/10.1016/j.gca.2018.03.009>
- Oran, R., Weiss, B. P., De Soria Santacruz-Pich, M., Jun, I., Lawrence, D. J., Polanskey, C. A., et al. (2022). Maximum energies of trapped particles around magnetized planets and small bodies. *Geophysical Research Letters*, 49(13), e2021GL097014. <https://doi.org/10.1029/2021gl097014>
- Plotkin, H., Clarke, R. S., Jr., McCoy, T. J., & Corrigan, C. M. (2012). The Old Woman, California, IAB iron meteorite. *Meteoritics & Planetary Science*, 47(5), 929–946. <https://doi.org/10.1111/j.1945-5100.2012.01348.x>
- Polanskey, C. A., Elkins-Tanton, L., Jaumann, R., Lawrence, D. J., Marsh, D. M., Moore, R. R., et al. (2018). Psyche science operations concept: Maximize reuse to minimize risk. In *2018 SpaceOps Conference*. American Institute of Aeronautics and Astronautics.
- Richter, I., Auster, H. U., Glassmeier, K. H., Koenders, C., Carr, C. M., Motschmann, U., et al. (2012). Magnetic field measurements during the ROSETTA flyby at asteroid (21)Lutetia. *Planetary and Space Science*, 66(1), 155–164. <https://doi.org/10.1016/j.pss.2011.08.009>
- Richter, I., Brinza, D. E., Cassel, M., Glassmeier, K.-H., Kuhnke, F., Musmann, G., et al. (2001). First direct magnetic field measurements of an asteroidal magnetic field: DS1 at Braille. *Geophysical Research Letters*, 28(10), 1913–1916. <https://doi.org/10.1029/2000gl012679>
- Scheinberg, A., Fu, R. R., & Weiss, B. P. (2015). Asteroid differentiation: Melting and large-scale structure. In P. Michel, F. E. De Meo, & W. F. Bottke (Eds.), *Asteroids IV* (pp. 533–552). University of Arizona Press.
- Shah, J., Bates, H. C., Muxworthy, A. R., Hezel, D. C., Russell, S. S., & Genge, M. J. (2017). Long-lived magnetism on chondrite parent bodies. *Earth and Planetary Science Letters*, 475, 106–118. <https://doi.org/10.1016/j.epsl.2017.07.035>
- Terho, M., Pesonen, L. J., & Kukkonen, I. T. (1993). *Petrophysical classification of meteorites: New results* (pp. 1–68). Geological Survey of Finland. Q29.1/91/1.
- Uehara, M., Gattacceca, J., Leroux, H., Jacob, D., & van der Beek, C. J. (2011). Magnetic microstructures of metal grains in equilibrated ordinary chondrites and implications for paleomagnetism of meteorites. *Earth and Planetary Science Letters*, 306(3), 241–252. <https://doi.org/10.1016/j.epsl.2011.04.008>
- Vervelidou, F., Weiss, B. P., & Lagroix, F. (2023). Hand magnets and the destruction of ancient meteorite magnetism. *Journal of Geophysical Research: Planets*, 128(4), e2022JE007464. <https://doi.org/10.1029/2022je007464>

- Wasilewski, P. J., Acuna, M. H., & Kletetschka, G. (2002). 433 Eros: Problems with the meteorite magnetism record in attempting an asteroid match. *Meteoritics & Planetary Science*, *37*, 937950.
- Wasilewski, P. J., Dickinson, T. L., Connerney, J. E., & Funaki, M. (1997). Asteroid magnetic records - Possible insight from the analysis of large meteorites. In *Presented at the Antarctic meteorites XXII* (pp. 203–207).
- Weiss, B. P., Gattacceca, J., Stanley, S., Rochette, P., & Christensen, U. R. (2010). Paleomagnetic records of meteorites and early planetesimal differentiation. *Space Science Reviews*, *152*(1), 341–390. <https://doi.org/10.1007/s11214-009-9580-z>
- Weiss, B. P., Merayo, J. M. G., Ream, J. B., Oran, R., Brauer, P., Cochrane, C. J., et al. (2023). The Psyche magnetometry investigation. *Space Science Reviews*, *219*(3), 22. <https://doi.org/10.1007/s11214-023-00965-z>
- Yang, J., & Goldstein, J. I. (2006). Metallographic cooling rates of the IIIAB iron meteorites. *Geochimica et Cosmochimica Acta*, *70*(12), 3197–3215. <https://doi.org/10.1016/j.gca.2006.04.007>
- Yu, Y., & Tauxe, L. (2006). Acquisition of viscous remanent magnetization. *Physics of the Earth and Planetary Interiors*, *159*(1), 32–42. <https://doi.org/10.1016/j.pepi.2006.05.002>